IET Systems Biology

Research Article

IET Journals
The Institution of Engineering and Technology

Crosstalk between pathways enhances the controllability of signalling networks

ISSN 1751-8849
Received on 28th December 2014
Revised on 24th February 2015
Accepted on 27th February 2015
doi: 10.1049/iet-syb.2014.0061
www.ietdl.org

Dingjie Wang, Suoqin Jin, Xiufen Zou ✉

School of Mathematics and Statistics, Wuhan University, Wuhan 430072, People's Republic of China
✉ *E-mail: xfzou@whu.edu.cn*

Abstract: The control of complex networks is one of the most challenging problems in the fields of biology and engineering. In this study, the authors explored the controllability and control energy of several signalling networks, which consisted of many interconnected pathways, including networks with a bow-tie architecture. On the basis of the theory of structure controllability, they revealed that biological mechanisms, such as cross-pathway interactions, compartmentalisation and so on make the networks easier to fully control. Furthermore, using numerical simulations for two realistic examples, they demonstrated that the control energy of normal networks with crosstalk is lower than in networks without crosstalk. These results indicate that the biological networks are optimally designed to achieve their normal functions from the viewpoint of the control theory. The authors' work provides a comprehensive understanding of the impact of network structures and properties on controllability.

1 Introduction

The control of complex networks is one of the most challenging problems in modern network science and engineering. Although great effort has been devoted to understanding the interplay between complex networks and the dynamic processes that take place within them in various natural and technological systems [1–4], the control of complex dynamic networks remains an important problem.

Cell signalling is one part of a complex system of communication that governs basic cellular activities and coordinates cell actions. Owing to the complexity of cellular signalling networks, their control is very important. In many biological signal transduction pathways, multiple input signals converge on a shared set of signalling components, which route each input to the appropriate output [5, 6]. In other words, most signalling networks exhibit a bow-tie architecture: a huge number of inputs are converted to a small number of intermediates, which then fan out to generate a huge number of outputs. In a signalling network, complicated interactions exist among proteins, such as activation and inactivation, phosphorylation and dephosphorylation, dissociation and degradation, and so on. Moreover, a crosstalk between different pathways exists, and these complex interactions and crosstalking make the dynamics of the networks complicated. Although much progress has been made on the structural controllability theory and network dynamics [7–12], the exploration of the relationships between the controllability of signalling networks and the architecture based on the network dynamics is lacking. Therefore in this study, we focused on investigating how the crosstalk mechanisms for signalling networks affect the controllability of the signalling networks and the control energy.

The paper is organised as follows. Section 2 provides the network model and some preliminary results. The design and analysis of the controllability of several simple signalling networks and complex networks with bow-tie architecture based on their dynamics are given in Sections 3 and 4, respectively. The application of our methodology to two realistic examples is shown in Section 5. Finally, some conclusions are addressed in Section 6.

2 Network model and mathematical preliminaries

2.1 Controllability of complex networks

Although most real systems are non-linear processes, the controllability of non-linear systems is in many respects structurally similar to that of linear systems [8, 9, 12, 13]. In this section, we introduce the notation, definitions and preliminary results regarding the controllability of complex networks.

Suppose that the dynamics of a network with n nodes can be described using the following time-invariant ordinary differential equations (ODEs)

$$\frac{\mathrm{d}\boldsymbol{x}(t)}{\mathrm{d}t} = \boldsymbol{A}\boldsymbol{x}(t) + \boldsymbol{B}\boldsymbol{u}(t) \tag{1}$$

Vector $\boldsymbol{x}(t) = (x_1(t), \ldots, x_N(t))^{\mathrm{T}}$ captures the states of the N nodes at time t. For example, $x_i(t)$ can denote the transcription factor concentration in a gene regulatory network. Matrix $\boldsymbol{A} \in R^{N\times N}$ denotes the coupling matrix of the system, which describes the strength of the system interactions of the links, and a_{ij} represents the weight of a directed link from node j to i. Matrix $\boldsymbol{B} \in R^{N\times M}$ is the control matrix, and $\boldsymbol{u}(t) = (u_1(t), \ldots, u_M(t))^{\mathrm{T}}$ is the vector of M controllers.

Definition 1: (*C*omplete controllability)*:* The network described by (1) is said to be completely controllable if it can be steered from any initial state to any desired final state in a finite time.

Theorem 1: (Kalman rank condition [*14*])*:* The system ($\boldsymbol{A}$, $\boldsymbol{B}$) is completely controllable if and only if

$$\mathrm{rank}[\boldsymbol{B}, \boldsymbol{A}\boldsymbol{B}, \ldots, \boldsymbol{A}^{N-1}\boldsymbol{B}] = N \tag{2}$$

To apply Theorem 1 to an arbitrary network, we need to know the weight of each link, but most real networks are either unknown or are only approximately known and are time dependent. Lin [15] proposed a structurally controllable notation.

Definition 2: (Structural controllability)*:* The system ($\boldsymbol{A}$, $\boldsymbol{B}$) is considered to be structurally controllable if it is possible to fix the free parameters in $\boldsymbol{A}$, $\boldsymbol{B}$ to certain values so that the obtained system ($\boldsymbol{A}$, $\boldsymbol{B}$) is controllable in the usual sense.

Definition 3: (Strong structural controllability)*:* The system ($\boldsymbol{A}$, $\boldsymbol{B}$) is referred to as having strong structural controllability if the system ($\boldsymbol{A}$, $\boldsymbol{B}$) is always controllable as long as every free parameter in $\boldsymbol{A}$, $\boldsymbol{B}$ is not zero.

According to the definitions, we can conclude that every strongly structurally controllable system is also structurally controllable, while the opposite is not true.

Definition 4: (Control energy)*:* The energy cost of the control input $\boldsymbol{u}(\boldsymbol{t})$ can be defined as

$$E(\boldsymbol{u}(\boldsymbol{t}), t_f) = \int_0^{t_f} \left\|\boldsymbol{u}(\boldsymbol{t})\right\|^2 \mathrm{d}t \tag{3}$$

2.2 Fixed-time minimum-energy controllability

For the N-dimensional linear time-invariant dynamics and given the certain initial state of $\boldsymbol{x}_0 = 0$ and the certain target state $\boldsymbol{x}_\mathrm{f}$, one method for evaluating the qualities of the controllability is to consider the fixed-time minimum-energy control problem. It can be defined as follows [16]

$$\begin{aligned} &\min_{\boldsymbol{u}(\boldsymbol{t})\in L_2} \int_0^{t_\mathrm{f}} \left\|\boldsymbol{u}(\boldsymbol{t})\right\|^2 \mathrm{d}t \\ &\text{subject to } \begin{cases} \dot{\boldsymbol{x}}(\boldsymbol{t}) = \boldsymbol{A}\boldsymbol{x}(\boldsymbol{t}) + \boldsymbol{B}\boldsymbol{u}(\boldsymbol{t}) \\ \boldsymbol{x}(0) = 0, \quad \boldsymbol{x}(\boldsymbol{t}_\mathrm{f}) = \boldsymbol{x}_\mathrm{f}, \ [0, t_\mathrm{f}] \ \text{ fixed} \end{cases} \end{aligned} \tag{4}$$

If the system is completely controllable, then the minimum control energy is given by

$$\int_0^{t_\mathrm{f}} \left\|\boldsymbol{u}^*(\boldsymbol{t})\right\|^2 \mathrm{d}t = \boldsymbol{x}_\mathrm{f}^{\boldsymbol{T}} \boldsymbol{W}_{t_\mathrm{f}}^{-1} \boldsymbol{x}_\mathrm{f} \tag{5}$$

where the matrix $\boldsymbol{W}_{t_\mathrm{f}} = \int_0^{t_\mathrm{f}} \mathrm{e}^{\boldsymbol{A}t} \boldsymbol{B}\boldsymbol{B}^{\boldsymbol{T}} \mathrm{e}^{\boldsymbol{A}^{\boldsymbol{T}}\mathrm{t}} \mathrm{d}t$ is referred to as the Gramian matrix at time t_f, and the optimal control input has the following form

$$\boldsymbol{u}^*(\boldsymbol{t}) = \boldsymbol{B}^{\boldsymbol{T}} \mathrm{e}^{\boldsymbol{A}^{\boldsymbol{T}}(t_\mathrm{f}-t)} \boldsymbol{W}_{t_\mathrm{f}}^{-1} \boldsymbol{x}_\mathrm{f} \tag{6}$$

The Gramian matrix is positive semi-definite and has the same rank as [$\boldsymbol{B}$, $\boldsymbol{AB}$, …, $\boldsymbol{A}^{N-1}\boldsymbol{B}$].

2.3 Energy-related controllability metric

The controllability criteria, such as the Kalman rank condition [14], only provides an answer to the binary question of whether the system is controllable or not, but it does not associate with or identify the degree of the quality of controllability. Muller [17] proposed three energy-related controllability metrics: the trace, determinant and maximum eigenvalue of the inverse characteristic Gramian matrix. Here, we focused on the first metric, namely the trace of the inverse characteristic Gramian matrix. This metric is given by the average value of the minimum control energy over the unit hypersphere $\{\boldsymbol{x}:\|\boldsymbol{x}\| = 1\}$

$$\bar{E}(\boldsymbol{u}^*, t_\mathrm{f}) = \frac{\int_{\|\boldsymbol{x}\|=1} \boldsymbol{x}^{\boldsymbol{T}} \boldsymbol{W}_{t_\mathrm{f}}^{-1} \boldsymbol{x} \, \mathrm{d}\boldsymbol{x}}{\int_{\|\boldsymbol{x}\|=1} \mathrm{d}\boldsymbol{x}} \tag{7}$$

which is calculated as

$$\bar{E}(\boldsymbol{u}^*, t_\mathrm{f}) = \frac{1}{n} \mathrm{tr}\, \boldsymbol{W}_{t_\mathrm{f}}^{-1} \tag{8}$$

For practical applications, it is desirable to keep the average costs (8) as small as possible. In this study, we use this average energy to quantify the energy needed to control the network.

3 Controllability of several simple signalling networks

3.1 Basic signalling network with shared elements

We begin with the simplest model of a multi-layered network. That is, a simple signalling network is composed of two signalling pathways, X and Y, which are initiated by the signals $x_0(t)$ and $y_0(t)$, respectively (Fig. 1) [18, 19], and there are two outputs, x_2 and y_2.

The linear dynamics shown in Fig. 1 can be written as follows

$$\begin{cases} \dot{x}_1 = -d_1 x_1 + u(t) \\ \dot{x}_2 = a_2 x_1 - d_2^x x_2 \\ \dot{y}_2 = b_2 x_1 - d_2^y y_2 \end{cases} \tag{9}$$

where $u(t) = a_1 x_0(t) + b_1 y_0(t)$ is the input signals or control function. The coupling matrix in (9) can be written as

$$\boldsymbol{A} = \begin{bmatrix} -d_1 & 0 & 0 \\ a_2 & -d_2^x & 0 \\ b_2 & 0 & -d_2^y \end{bmatrix} \tag{10}$$

where $\boldsymbol{B} = \begin{bmatrix} 1 & 0 & 0 \end{bmatrix}^{\mathrm{T}}$ and the controllability matrix $\boldsymbol{C}$ is given by

$$\boldsymbol{C} = [\boldsymbol{B}, \boldsymbol{AB}, \boldsymbol{A}^2\boldsymbol{B}] = \begin{bmatrix} 1 & -d_1 & d_1^2 \\ 0 & a_2 & -a_2(d_1 + d_2^x) \\ 0 & b_2 & -b_2(d_1 + d_2^y) \end{bmatrix} \tag{11}$$

When $d_2^x = d_2^y$, then $\mathrm{rank}(\boldsymbol{C}) = 2 < N$ and the system will be uncontrollable. This result shows that the decay constants affect the controllability in the simplest networks.

3.2 Effects of crosstalk on the controllability of signalling networks

3.2.1 Inhibition between pathways: Real cellular signalling networks that share components feature various elaborations, or embellishments. Cross-pathway inhibition (Fig. 2) occurs when a downstream component of pathway X inhibits a downstream component of pathway Y [18, 19].

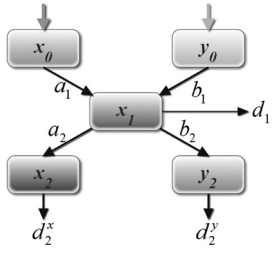

Fig. 1 *Basic network architecture with shared element x_1.$x_0(t)$ and $y_0(t)$ are input signals*

Parameters a_1, a_2, b_1 and b_2 are activation rate constants, and d_1, $d_2{}^x$ and $d_2{}^y$ are inactivation or decay rate constants

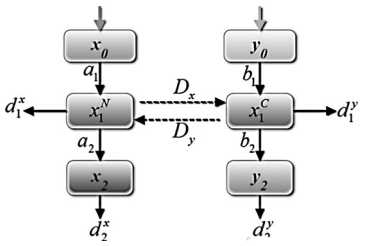

Fig. 2 *Network with cross-pathway inhibition*

The linear dynamics shown in Fig. 2 can be written as

$$\begin{cases} \dot{x}_1 = -d_1 x_1 + u(t) \\ \dot{x}_2 = a_2 x_1 - d_2^x x_2 \\ \dot{y}_2 = b_2 x_1 - g x_2 - d_2^y y_2 \end{cases} \tag{12}$$

We then obtain the coupling matrix and the control matrix

$$\boldsymbol{A} = \begin{bmatrix} -d_1 & 0 & 0 \\ a_2 & -d_2^x & 0 \\ b_2 & -g & -d_2^y \end{bmatrix}, \quad \boldsymbol{B} = \begin{bmatrix} 1 \\ 0 \\ 0 \end{bmatrix}$$

and the controllability matrix is given by

$$\boldsymbol{C} = [\boldsymbol{B}, \boldsymbol{AB}, \boldsymbol{A}^2\boldsymbol{B}] = \begin{bmatrix} 1 & -d_1 & d_1^2 \\ 0 & a_2 & -a_2(d_1 + d_2^x) \\ 0 & b_2 & -(b_2 d_1 + b_2 d_2{}^y + a_2 g) \end{bmatrix}$$

We can easily obtain rank($\boldsymbol{C}$) = 3 = N. Therefore the system is strongly structurally controllable when only controlling the shared element x_1. This result indicates that the controllability will be not affected by the decay constants because of cross-pathway inhibition in the networks. In other words, the cross-pathway inhibition enhances the controllability of the networks.

We will take this network as an example to perform the simulations. The parameters are generated randomly in (0, 1), and the control function is computed using the method in [20]. The numerical results show that all of the stated variables can be controlled to the origin using our theoretical results (Fig. 3).

3.2.2 Networks with two insulating mechanisms: compartmentalisation and the action of a scaffold protein: Real cellular signalling networks that share components typically contain one or more insulating mechanisms that are

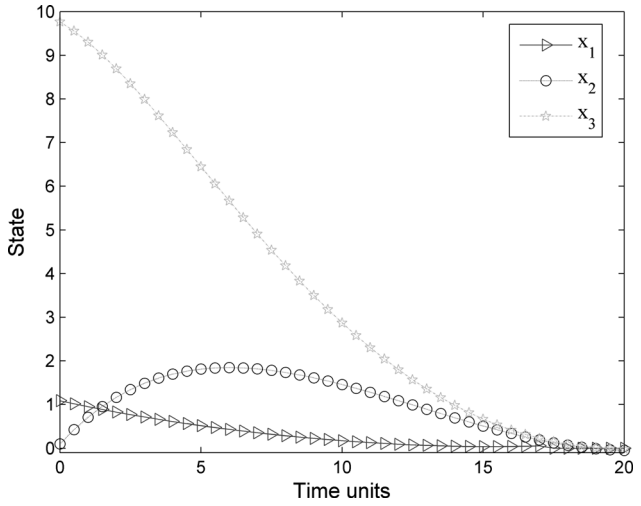

Fig. 3 *Numerical simulations of the dynamic model (12)*

Fig. 4 *Networks with compartmentalisation or scaffolding*

thought to contribute to the specificity and fidelity [18, 21]. In compartmentalisation, different pathways are localised to different cellular compartments or to different spatial locations within the cell (Fig. 4) [22]. The extent of leakage between the two pathways is determined by the efficiency of the compartmentalisation. For example, assume that the pathway-specific components of pathway X are localised to the nucleus, while those of pathway Y are localised to the cytosol. Although the shared kinase, x_1, is found in both compartments (x_1^{N} is the nuclear pool and x_1^{C} is the cytosolic pool), x_1, which is activated by the input signal x_0 in the nucleus, is likely to encounter target x_2, which is also in the nucleus; it will only encounter target y_2 if it diffuses into the cytosol before it is deactivated. Therefore crossover between the two pathways occurs when kinase x_1 leaks into or out of the nucleus. D_x is the coefficient for the rate at which x_1 exits the nucleus and enters the cytosol, and D_y is the rate constant for x_1 leaving the cytosol and entering the nucleus. D_x and D_y can be considered to be pseudo-diffusion rate constants or exchange rate constants. The parameters d_1^x and d_1^y are the deactivation constants for x_1 in the nucleus and cytosol, respectively. The parameters d_2^x and d_2^y are the deactivation constants for x_2 and y_2, respectively.

The linear dynamics shown in Fig. 4 can be written as

$$\begin{cases} \dot{x}_1^{\mathrm{N}} = -\left(D_x + d_1^x\right)x_1^{\mathrm{N}} + D_y x_1^{\mathrm{C}} + c_1 u_1^{\mathrm{N}}(t) \\ \dot{x}_1^{\mathrm{C}} = D_x x_1^{\mathrm{N}} - \left(D_y + d_1^y\right)x_1^{\mathrm{C}} + c_2 u_1^{\mathrm{C}}(t) \\ \dot{x}_2 = a_2 x_1^{\mathrm{N}} - d_2^x x_2 \\ \dot{y}_2 = b_2 x_1^{\mathrm{C}} - d_2^y y_2 \end{cases} \tag{13}$$

where $u_1^{\mathrm{N}}(t) = a_1 x_0(t)$ and $u_1^{\mathrm{C}}(t) = b_1 y_0(t)$ are the input signals or control functions.

The coupling matrix can be written as

$$\boldsymbol{A} = \begin{bmatrix} -(D_x + d_1^x) & D_y & 0 & 0 \\ D_x & -(D_y + d_1^y) & 0 & 0 \\ a_2 & 0 & -d_2^x & 0 \\ 0 & b_2 & 0 & -d_2^y \end{bmatrix}$$

When $\boldsymbol{B} = \begin{bmatrix} 1 & 0 & 0 & 0 \\ 0 & 1 & 0 & 0 \end{bmatrix}^{\mathrm{T}}$, the controllability matrix $\boldsymbol{C}$ is given as follows (see equation at the bottom of the next page)

We easily find that rank($\boldsymbol{C}$) = 4 = N. Therefore the system is strongly structurally controllable by only controlling the shared element x_1.

4 Controllability of bow-tie signalling networks

A bow-tie or hourglass structure is a common architectural feature found in biological and technological networks, especially in metabolic and signalling networks [23, 24].

4.1 Simplest bow-tie structure

A bow-tie in a multi-layered network means that the network is capable of processing many different inputs, by converting them into a small set of universal building blocks and then re-using

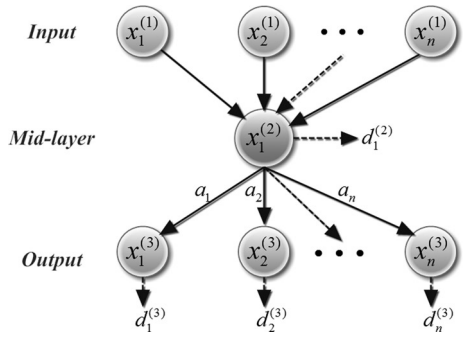

Fig. 5 *Simplest three-layered bow-tie signalling network [23]*

these building blocks to construct a wide range of outputs. In Fig. 5, we illustrate several networks with three layers of nodes. There are M input signals $x_j^{(1)}(j = 1, 2, \ldots, M)$, only one shared element $x_j^{(2)}$ and N outputs signals $x_j^{(3)}(j = 1, 2, \ldots, N)$ [20].

The linear dynamics shown in Fig. 5 can be written as

$$\begin{cases} \dot{x}_1^{(2)} = -d_1^{(2)} x_1^{(2)} + u(t) \\ \dot{x}_i^{(3)} = a_i x_1^{(2)} - d_i^{(3)} x_i^{(3)}, \quad i = 1, \ldots, N \end{cases} \tag{14}$$

where $u(t) = \sum_{j=1}^{M} b_j x_j^{(1)}$ is the input signal or control function. The coupling matrix can be written as

$$\boldsymbol{A} = \begin{bmatrix} -d_1^{(2)} & 0 & 0 & 0 & 0 \\ a_1 & -d_1^{(3)} & 0 & 0 & 0 \\ a_2 & 0 & -d_2^{(3)} & 0 & 0 \\ \vdots & \vdots & \vdots & \ddots & \vdots \\ a_n & 0 & 0 & 0 & -d_N^{(3)} \end{bmatrix}$$

When $\boldsymbol{B} = \begin{bmatrix} 1 & 0 & \cdots & 0 \end{bmatrix}_{N\times 1}^{\mathrm{T}}$, we obtain the following controllability matrix $\boldsymbol{C}$.

$$\boldsymbol{C} = [\boldsymbol{B}, \boldsymbol{AB}, \ldots, \boldsymbol{A}^{N-1}\boldsymbol{B}]$$

$$= \begin{bmatrix} 1 & -d_1 & d_1^2 & \cdots & (-1)^{N-1} d_1^{N-1} \\ 0 & a_2 & -a_2(d_1 + d_2) & \cdots & (-1)^N a_2 \sum_{i=0}^{N-2} d_1^{N-2-i} d_2^i \\ 0 & a_3 & -a_3(d_1 + d_3) & \cdots & (-1)^N a_3 \sum_{i=0}^{N-2} d_1^{N-2-i} d_3^i \\ \vdots & \vdots & \vdots & \vdots & \vdots \\ 0 & a_N & -a_N(d_1 + d_N) & \cdots & (-1)^N a_N \sum_{i=0}^{N-2} d_1^{N-2-i} d_N^i \end{bmatrix}$$

We easily find that $\mathrm{rank}(\boldsymbol{C}) \le N - 1 < N$ when $d_i = d_j$ $(i \neq j, 2 \le i, j \le N)$. Therefore the system will be uncontrollable. In other cases, rank

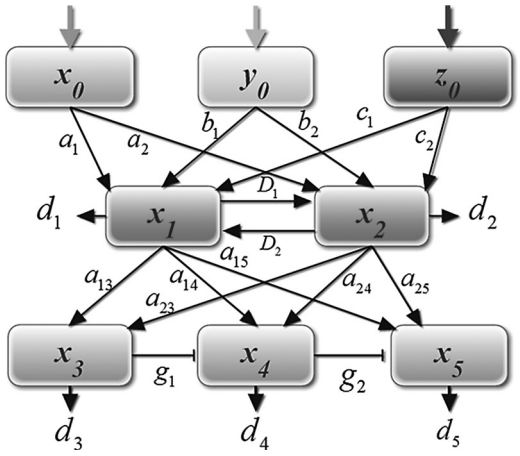

Fig. 6 *Bow-tie three-layered signalling network with cross-pathway inhibition*

$(\boldsymbol{C}) = N$ and the system will be controllable. Taken together, the system is structurally controllable, but not strongly structurally controllable.

4.2 Bow-tie structure with cross-inhibition pathways

The linear dynamics shown in Fig. 6 can be written as

$$\begin{cases} \dot{x}_1 = D_2 x_2 - d_1 x_1 + u_1(t) \\ \dot{x}_2 = D_1 x_1 - d_2 x_2 + u_2(t) \\ \dot{x}_3 = a_{13} x_1 + a_{23} x_2 - d_3 x_3 \\ \dot{x}_4 = a_{14} x_1 + a_{24} x_2 - g_1 x_3 - d_4 x_4 \\ \dot{x}_5 = a_{15} x_1 + a_{25} x_2 - g_2 x_4 - d_5 x_5 \end{cases} \tag{15}$$

where $u_1(t) = a_1 x_0 + b_1 y_0 + c_1 z_0$, $u_2(t) = a_2 x_0 + b_2 y_0 + c_2 z_0$ are the input signals or control functions. When $\boldsymbol{B} = \begin{bmatrix} 1 & 0 & 0 & 0 & 0 \\ 0 & 1 & 0 & 0 & 0 \end{bmatrix}^{\mathrm{T}}$, the controllability matrix $\boldsymbol{C}$ is given as follows (see equation at the bottom of the next page)

We find that this system is strongly structurally controllable because of $\mathrm{rank}(\boldsymbol{C}) = 5 = N$. Compared with the system (14), our findings show that cross-inhibitions enhance the controllability of bow-tie signalling networks.

5 Application using realistic examples

To validate our results, we investigated the controllability of two realistic biological systems from two different aspects. One example is the innate immune signalling network [25–27], and the other example is the cell-fate decision network [28–30].

$$\boldsymbol{C} = [\boldsymbol{B}, \boldsymbol{AB}, \boldsymbol{A}^2\boldsymbol{B}, \boldsymbol{A}^3\boldsymbol{B}] \triangleq \begin{bmatrix} \boldsymbol{C}_1 & \boldsymbol{C}_2 & \boldsymbol{C}_3 & \boldsymbol{C}_4 \end{bmatrix}$$

$$\boldsymbol{C}_1 = \begin{bmatrix} 1 & 0 & 0 & 0 \\ 0 & 1 & 0 & 0 \end{bmatrix}^{\mathrm{T}}, \quad \boldsymbol{C}_2 = \begin{bmatrix} -(D_x + d_1^x) & D_x & a_2 & 0 \\ D_y & -(D_y + d_1^y) & 0 & b_2 \end{bmatrix}^{\mathrm{T}}$$

$$\boldsymbol{C}_3 = \begin{bmatrix} c_{31} & -D_x c_{32} & -a_2(d_1^x + d_2^x + D_x) & D_x b_2 \\ -D_y c_{32} & c_{33} & D_y a_2 & -b_2(d_2^y + d_1^y + D_y) \end{bmatrix}^{\mathrm{T}}$$

$$c_{31} = (D_x + d_1^x)^2 + D_x D_y, \quad c_{32} = D_x + D_y + d_1^x + d_1^y$$

$$c_{33} = (D_y + d_1^y)^2 + D_x D_y, \quad C_4 \in R^{4\times 2}$$

5.1 Innate immune signalling network

The innate immune response is important for the regulation of pathogen infections because most infectious pathogens are eliminated through the innate immune response without necessarily requiring the activation of adaptive immunity [25]. Viruses are a major pathogen in both humans and animals. In response to a viral infection, dsRNA interacts with the RNA helicase domain of RIG-I or MAD5, which transmits signals to phosphorylate MITA. The phosphorylated MITA activates TBK1, leading to the phosphorylation of IRF3 and IRF7. In addition, phosphorylated MITA induces the activation of NF-κB via the IKK proteins. The activated NF-κB and phosphorylated IRF3 and IRF7 are translocated to the nucleus to trigger IFN mRNA induction, which leads to the production of type I IFNs (IFN-α and IFN-β). The type I IFNs induce the transcription of IFN-stimulated genes, such as ISG56; some antiviral proteins and IRF7 are also induced by IFN-mediated signalling pathways. The induced ISG56 inhibits the activation of MITA and TBK1, and the antiviral proteins inhibit the viral replication by targeting the viral RNA [25, 26, 31]. The simplified diagram of the virus-induced type I IFN signalling pathways is presented in Fig. 7, which consists of ten nodes.

There are four cross-pathway interactions in this network, including AVP —| virus, ISG56 —| MITA, ISG56 —| TBK1 and IFN-β→IRF7. The linear dynamics shown in Fig. 7 can be formulated as

$$\begin{cases} \dot{x}_1 = a_{1,1}x_1 - a_{1,10}x_{10} - d_1x_1 \\ \dot{x}_2 = a_{2,1}x_1 - a_{2,9}x_9 - d_2x_2 \\ \dot{x}_3 = a_{3,2}x_2 - d_3x_3 \\ \dot{x}_4 = a_{4,3}x_3 - d_4x_4 \\ \dot{x}_5 = a_{5,2}x_2 - a_{5,9}x_9 - d_5x_5 \\ \dot{x}_6 = a_{6,5}x_5 - d_6x_6 \\ \dot{x}_7 = a_{7,5}x_5 + a_{7,8}x_8 - d_8x_8 \\ \dot{x}_8 = a_{8,4}x_4 + a_{8,6}x_4 + a_{8,7}x_4 - d_8x_8 + u(t) \\ \dot{x}_9 = a_{9,8}x_8 - d_9x_9 \\ \dot{x}_{10} = a_{10,8}x_8 - d_{10}x_{10} \end{cases} \tag{16}$$

which can be written as

$$\dot{x} = Ax + Bu \tag{17}$$

where $x = (x_1, x_2, ..., x_N)^{\mathrm{T}}$ represents the states of the nodes, and x_i represents the concentration of the virus, MITA, IKK, NF-κB, TBK1, IRF3, IRF7, IFN-β, ISG56 and AVP. $a_{i,j}$ indicates the interaction strength from node j to i, and d_i is the degradation rate. $\boldsymbol{A} \in \boldsymbol{R}^{N\times N}$ denotes the coupling matrix of the system, where the diagonal element is $-d_i$, with the exception of the first element, which is $a_{11} - d_1$. $u(t)$ is the control function, and $\boldsymbol{B}$ is the control matrix.

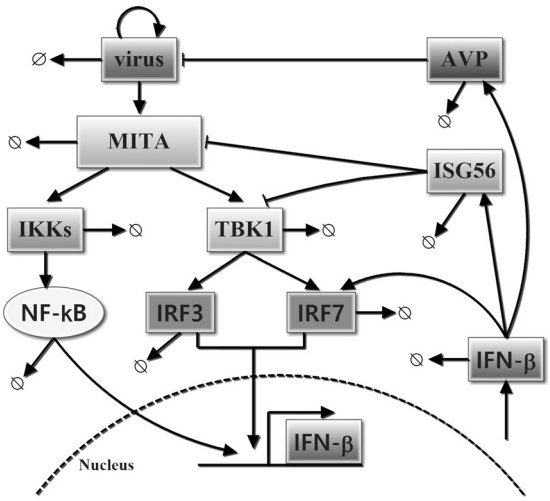

Fig. 7 *Simplified diagram of virus-induced type I IFN signalling pathways network [25]*

We investigated the controllability of this network using the maximum multiplicity theory (MMT) [9] by assigning each parameter a random weight. We found that the minimum driver node is 1 for the network either with or without crosstalk interactions, which is consistent with the results determined according to the maximum matching algorithm [7]. In the implementation of the maximum matching algorithm, we considered the degradation term as a self-loop for each node. Using the well-known Hopcroft–Karp algorithm [32], we showed that the network both with and without crosstalk interactions matched perfectly. In this case, any single node can be the driver node. We focused on IFN-β as the driver node, because of its critical role in the viral-induced immune response [26, 31]. When we controlled IFN-β, we found that the rank of the controllability matrix was 10 (fully ranked), while the rank of the controllability matrix was 3 (not fully ranked) if the four cross-pathway

$$\boldsymbol{C} = [\boldsymbol{B}, \boldsymbol{AB}, \boldsymbol{A}^2\boldsymbol{B}, \boldsymbol{A}^3\boldsymbol{B}, \boldsymbol{A}^4\boldsymbol{B}] \triangleq \begin{bmatrix} \boldsymbol{C}_1 & \boldsymbol{C}_2 & \boldsymbol{C}_3 & \boldsymbol{C}_4 & \boldsymbol{C}_5 & \boldsymbol{C}_6 & \boldsymbol{C}_7 & \boldsymbol{C}_8 \end{bmatrix}$$

$$\boldsymbol{C}_1 = \begin{bmatrix} 1 & 0 & 0 & 0 & 0 \end{bmatrix}^{\mathrm{T}}, \quad \boldsymbol{C}_2 = \begin{bmatrix} 0 & 1 & 0 & 0 & 0 \end{bmatrix}^{\mathrm{T}}$$

$$\boldsymbol{C}_3 = \begin{bmatrix} -d_1 & D_1 & a_{13} & a_{14} & a_{15} \end{bmatrix}^{\mathrm{T}}, \quad \boldsymbol{C}_4 = \begin{bmatrix} D_2 & -d_2 & a_{23} & a_{24} & a_{25} \end{bmatrix}^{\mathrm{T}}$$

$$\boldsymbol{C}_5 = \begin{bmatrix} d_1^{\,2} + D_1D_2 \\ -D_1(d_1 + d_2) \\ a_{23}D_1 - a_{13}(d_1 + d_3) \\ a_{24}D_1 - a_{14}(d_1 + d_4) - a_{13}g_1 \\ a_{25}D_1 - a_{15}(d_1 + d_5) - a_{14}g_2 \end{bmatrix}, \boldsymbol{C}_6 = \begin{bmatrix} -D_2(d_1 + d_2) \\ d_2^{\,2} + D_1D_2 \\ a_{13}D_2 - a_{23}(d_2 + d_3) \\ a_{14}D_2 - a_{24}(d_2 + d_4) - a_{23}g_1 \\ a_{15}D_2 - a_{25}(d_2 + d_5) - a_{24}g_2 \end{bmatrix}$$

$$\boldsymbol{C}_7 = \begin{bmatrix} -D_1D_2(d_1 + d_2) - d_1(d_1^{\,2} + D_1D_2) \\ d_2D_1(d_1 + d_2) + D_1(d_1^{\,2} + D_1D_2) \\ d_3(a_{13}d_1 - D_1a_{23} + a_{13}d_3) - a_{23}D_1(d_1 + d_2) + a_{13}(d_1^2 + D_1D_2) \\ g_1(a_{13}d_1 - D_1a_{23} + a_{13}d_3) - a_{24}D_1(d_1 + d_2) + a_{14}(d_1^{\,2} + D_1D_2) \\ +d_4(a_{14}(d_1 + d_4) - D_1a_{24} + a_{13}g_1) \\ d_5(a15(d_1 + d_5) - D_1a_{25} + a_{14}g_2) - a_{25}D_1(d_1 + d_2) + \\ g_2(a_{14}(d_1 + d_4) - D_1a_{24} + a_{13}g_1) + a_{15}(d_1^{\,2} + D_1D_2) \end{bmatrix}$$

$$\boldsymbol{C}_8 \in R^{5\times 3}$$

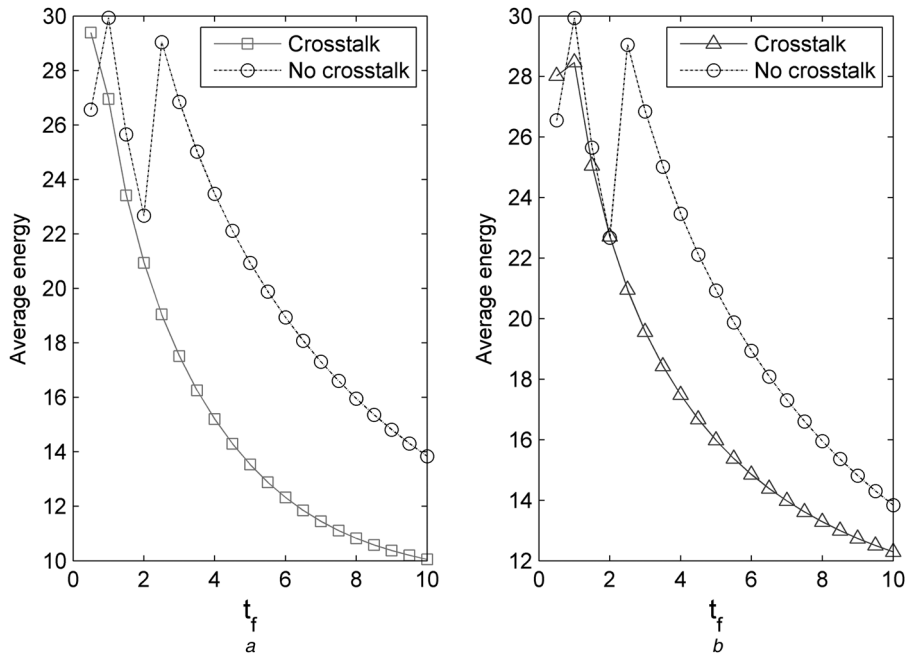

Fig. 8 *Comparison of the average energy between the network with crosstalk and that without it over the time t_f*

a Solid line indicates the average energy needed to completely control the network with the four cross-pathway interactions, and dashed line represents the results of the network without the four cross-pathway interactions

b Numerical results for the network with the four activation interactions between pathways and that without them

Average energy is the value by evaluating the natural logarithm. We assign each parameter a random value for the coupling matrix $\boldsymbol{A}$ of the system to calculate the average energy. In this figure, the parameters are set as follows: $a_{1,10} = 0.0464$, $a_{2,1} = 0.7719$, $a_{2,9} = 0.6311$, $a_{3,2} = 0.3883$, $a_{4,3} = 0.2290$, $a_{5,2} = 0.4845$, $a_{5,8} = 0.8258$, $a_{6,5} = 0.7819$, $a_{7,5} = 0.2941$, $a_{7,8} = 0.0484$, $a_{8,4} = 0.5309$, $a_{8,6} = 0.0915$, $a_{8,7} = 0.4053$, $a_{9,8} = 0.1123$, $a_{10,8} = 0.2916$, $a_{1,1} - d_1 = 0.0867$, $d_2 = 0.2057$, $d_3 = 0.5518$, $d_4 = 0.6419$, $d_5 = 0.1518$, $d_6 = 0.1006$, $d_7 = 0.2374$, $d_8 = 0.1048$, $d_9 = 0.7844$ and $d_{10} = 0.6053$

interactions were not present. Therefore the actual network is strongly structurally controllable, while the network without cross-pathway interactions is structurally controllable, but not strongly structurally controllable, suggesting that crosstalk can enhance the controllability of signalling networks.

Conversely, to specify the qualities of controllability, we calculated the average energy using metric (8). To perform an analysis of the average energy, the network should be completely controllable. Therefore we chose two driver nodes, namely the virus and IFN-β, to make the system satisfy the Kalman rank condition. We assigned each parameter a random value for the coupling matrix $\boldsymbol{A}$ of the system. The numerical results showed that the control of the network requires less energy than the control of the network without the four cross-pathway interactions (Fig. 8*a*). These results further demonstrate that the biological mechanisms make it easier to fully control the networks.

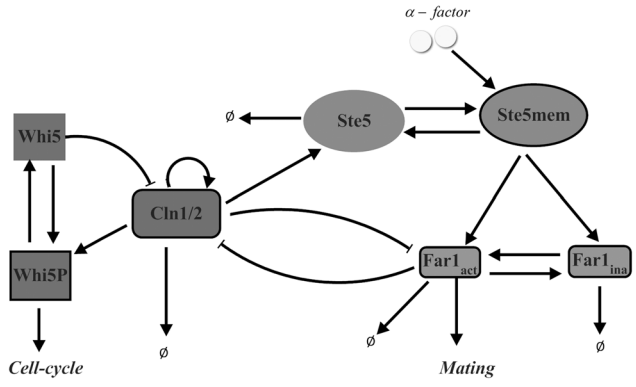

Fig. 9 *Schematic diagram of the core interacting network between the cell-cycle commitment and the mating arrest for cell-fate decision in budding yeast [29]*

To further investigate whether activation interactions between pathways can also allow networks to be controlled with less energy, we assumed the interactions, including AVP and the virus, ISG56 and MITA, and ISG56 and TBK1, to be activation interactions. The numerical results confirmed our hypothesis (Fig. 8*b*). We observed that the network uses less energy than the network without the four activation interactions when the network is completely controllable. Taken together, our findings demonstrate that crosstalk, regardless of whether it is an inhibition interaction or an activation interaction, makes the network easier to control.

5.2 Cell-fate decision network

The selection of a cell's fate in response to internal and external stimuli is essential for the development of multicellular organisms. Therefore it is important to precisely understand how cell-fate decisions are made. The core interaction network between the cell-cycle commitment and the mating arrest pathway from cell-fate decisions in budding yeast has been constructed in [30]. This network includes two subsystems, namely the cell cycle subsystem and the pheromone-induced MAPK pathway subsystem. In budding yeast, cell cycle commitment is initiated by the G1 cyclin Cln3, which forms a complex with Cln3-Cdk to phosphorylate the transcriptional inhibitor Whi5. The phosphorylated Whi5P is removed from the nucleus, thus activating the transcription of two G1 cyclins (Cln1 and Cln2). Cln1/2-Cdk promotes its own accumulation by phosphorylating Whi5. When Cln1/2 is highly expressed, the majority of the Whi5 is phosphorylated and the cell can pass through the start point. The mating pathway is a MAPK cascade that primarily arrests the cell cycle prior to DNA replication. A pheromone (e.g. α-factor) binds to a G protein-coupled receptor at the plasma membrane (e.g. Ste2 for α-factor). The scaffold protein Ste5, which physically interacts with all three kinases (Ste11, Ste7 and Fus3), is necessary for the mating signalling. More detailed regulatory mechanisms have been presented in previous studies [27–30].

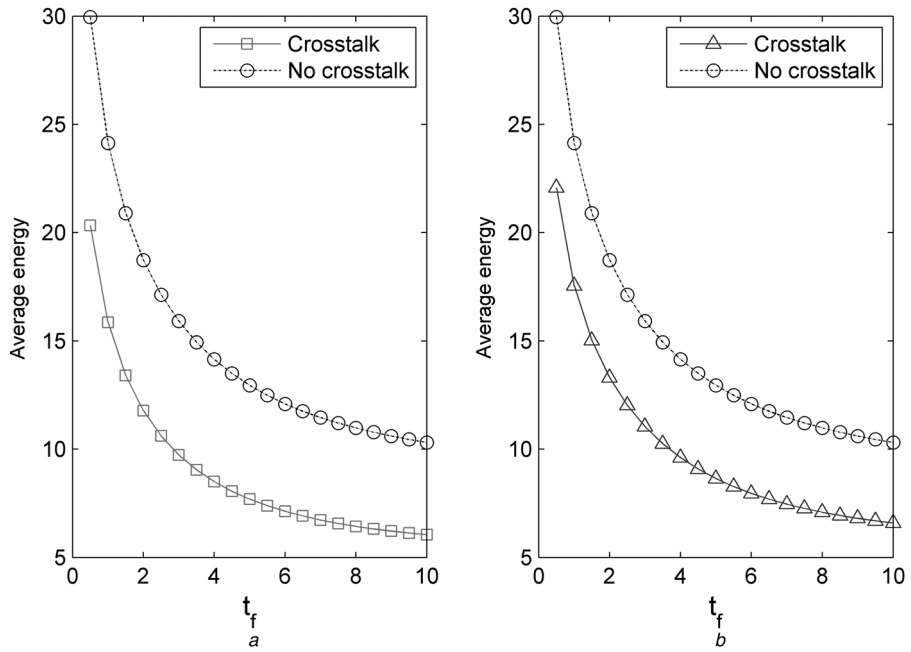

Fig. 10 *Comparison of the average energy between the network with crosstalk and that without it over the time t_f*

a Solid line indicates the average energy needed to completely control the network with the three cross-pathway interactions, and dashed line represents the results of the network without the three cross-pathway interactions

b Numerical results for the network with the three activation interactions between pathways and that without them

Average energy is the value by evaluating the natural logarithm. We assign each parameter a random value for the coupling matrix $\boldsymbol{A}$ of the system to calculate the average energy. In this figure, the parameters are set as follows: $a_{1,2} = 0.7447$, $a_{2,1} = 0.1890$, $a_{2,3} = 0.6868$, $a_{3,1} = 0.1835$, $a_{3,5} = 0.6443$, $a_{4,3} = 0.6256$, $a_{4,7} = 0.0811$, $a_{5,3} = 0.3786$, $a_{5,6} = 0.7757$, $a_{5,7} = 0.4868$, $a_{6,5} = 0.4359$, $a_{6,7} = 0.3063$, $a_{7,4} = 0.5085$, $a_{7,8} = 0.5108$, $a_{33} - d_3 = 0.3685$, $d_4 = 0.7802$, $d_5 = 0.9294$ and $d_6 = 0.4468$

Fig. 9 shows the simplified core interaction network between the cell cycle and the mating arrest pathways, which include eight nodes.

There are three cross-pathway interactions in this network, including Cln1/2—|Far1_{act}, Far1_{act}—|Cln1/2 and Cln1/2→Ste5_{mem}. The linear dynamics of this network can be formulated as

$$\begin{cases} \dot{x}_1 = a_{1,2}x_2 \\ \dot{x}_2 = a_{2,1}x_1 + a_{2,3}x_3 \\ \dot{x}_3 = -a_{3,1}x_1 + a_{33}x_3 - a_{3,5}x_5 - d_3x_3 \\ \dot{x}_4 = a_{4,3}x_3 + a_{4,7}x_7 - d_4x_4 \\ \dot{x}_5 = -a_{5,3}x_3 + a_{5,6}x_6 + a_{5,7}x_7 - d_5x_5 \\ \dot{x}_6 = a_{6,5}x_5 + a_{6,7}x_7 - d_6x_6 \\ \dot{x}_7 = a_{7,4}x_5 + a_{7,8}x_8 \\ \dot{x}_8 = u(t) \end{cases} \tag{18}$$

which can be written as

$$\dot{x} = Ax + Bu \tag{19}$$

where $x = (x_1, x_2, \ldots, x_N)^{\mathrm{T}}$ stands for the states of the nodes, and x_i ($i = 1, 2, \ldots, N$) represents the concentration of Whi5, Whi5p, Cln1/2, Ste5, Far1_{act}, Far_{ina}, Ste5mem and α-factor. $a_{i,\ j}$ indicates the interaction strength from node j to i, and d_i is the degradation rate. $\boldsymbol{A} \in \boldsymbol{R}^{N \times N}$ denotes the coupling matrix of the system, where the diagonal element is $-d_i$ or zero, with the exception of the third element, which is $a_{33} - d_3$. $u(t)$ is the control function, and $\boldsymbol{B}$ is the control matrix.

Using either the MMT [9] or the maximum matching algorithm [7], we identified that the minimum number of the driver node is 1 (α-factor) for the network without crosstalk interactions, which is the same as the network with crosstalk interactions. For any non-zero weights of $a_{i,j}$ and d_i, we found that the controllability matrix is always fully ranked when controlling α-factor. In other words, its controllability is independent of the detailed values of the parameters, indicating that the actual network is strongly structurally controllable. However, the rank of the controllability matrix is 5 (not fully ranked) if the 3 cross-pathway interactions are not present. Therefore these crosstalk mechanisms contribute to the controllability of the cell-fate decision network, which is consistent with the findings that crosstalk is required to ensure a successful switch between different cell fates [29, 30].

In addition, we selected two driver nodes, that is, Cln1/2 and α-factor, which make the system completely controllable, to calculate the average energy of the network according to (8). We also assigned a random value to each parameter. Fig. 10*a* shows that the control of the network requires less energy than the network without the three cross-pathway interactions. Therefore this example also indicates that the crosstalk between pathways makes it easier to fully control the networks.

To further investigate how activation crosstalk shapes the energy needed for controlling the networks, we assumed the interactions, including Cln1/2 and Far1_{act}, and Far1_{act} and Cln1/2, to be activation interactions. The numerical results revealed that the network requires less energy than the network without the three activation interactions when the network is completely controllable (Fig. 10*b*). Altogether, these results indicate that crosstalk, regardless of whether it is an inhibition interaction or an activation interaction, makes the network easier to control.

6 Concluding remarks

In this paper, we used the theory of structure controllability and system dynamics to analyse the controllability and control energy of different signalling networks. The results indicated that the structure and specific biological mechanisms of signalling networks determine the controllability. In particular, the intricate crosstalk is crucial for shaping the controllability of the signalling networks. These data will provide new insights into the optimal design of biological networks.

Owing to the ubiquity of non-linearity in nature, the control of complex networked systems with non-linear dynamics is important and cannot be ignored [33, 34]. Therefore the investigation of how non-linearity affects the global controllability and control energy will be the focus of future studies.

7 Acknowledgments

This work was supported by the Major Research Plan of the National Natural Science Foundation of China (no. 91230118), and the Chinese National Natural Science Foundation (no. 61173060) and the Fundamental Research Funds for the Central Universities (no. 2014201020201).

8 References

1 Newman, M.E.J.: 'The structure and function of complex networks', *SIAM Rev.*, 2003, **45**, (2), pp. 167–256
2 Boccaletti, S., Latora, V., Moreno, Y., *et al.*: 'Complex networks: structure and dynamics', *Phys. Rep.*, 2006, **424**, pp. 175–308
3 Jin, S., Li, Y., Pan, R., Zou, X.: 'Characterizing and controlling the inflammatory network during influenza A virus infection', *Sci. Rep.*, 2014, **4**, p. 3799
4 Wang, Y., Tan, J., Sadre-Marandi, F., *et al.*: 'Mathematical modeling for intracellular transport and binding of HIV-1 Gag proteins', *Math. Biosci.*, 2015, **262**, pp. 198–205
5 Liu, Z.P., Wang, Y., Zhang, X.S., *et al.*: 'Identifying dysfunctional crosstalk of pathways in various regions of Alzheimer's disease brains', *BMC Syst. Biol.*, 2010, **4**, Suppl 2, p. S11
6 Liu, Z.P., Zhang, W., Horimoto, K., *et al.*: 'Gaussian graphical model for identifying significantly responsive regulatory networks from time course high-throughput data', *IET Syst. Biol.*, 2013, **7**, pp. 143–152
7 Liu, Y.Y., Slotine, J.J., Barabasi, A.L.: 'Controllability of complex networks', *Nature*, 2011, **473**, (7346), pp. 167–173
8 Cowan, N.J., Chastain, E.J., Vilhena, D.A., *et al.*: 'Nodal dynamics, not degree distributions, determine the structural controllability of complex networks', *PLoS One*, 2012, **7**, (6), p. 38398
9 Yuan, Z., Zhao, C., Di, Z., *et al.*: 'Exact controllability of complex networks', *Nat. Commun.*, 2013, **4**, (2447), p. 3447
10 Wuchty, S.: 'Controllability in protein interaction networks', *Proc. Natl. Acad. Sci. USA*, 2014, **111**, (19), pp. 7156–7160
11 Ruths, J., Ruths, D.: 'Control profiles of complex networks', *Science*, 2014, **343**, (6177), pp. 1373–1376
12 Nepusz, T., Vicsek, T.: 'Controlling edge dynamics in complex networks', *Nat. Phys.*, 2012, **8**, pp. 568–573
13 Slotine, J.J., Li, W.: 'Applied nonlinear control' (Npnew Jersey Press, 1991)
14 Kalman, R.E.: 'Mathematical description of linear dynamical systems', *J. Soc. Ind. Appl. Math. Ser. A*, 1963, **1**, pp. 152–192
15 Lin, C.T.: 'Structural controllability', *IEEE Trans. Autom. Control*, 1974, **19**, pp. 201–208
16 Johnson, C.D.: 'Optimization of a certain quality of complete controllability and observability for linear dynamical systems', *J. Fluid Eng. – Trans. ASME*, 1969, **91**, (2), pp. 228–238
17 Muller, P.C.: 'Analysis and optimization of certain qualities of controllability and observability for linear dynamical systems', *Automatica*, 1972, **8**, (3), pp. 237–246
18 Komarova, N., Zou, X., Nie, Q., *et al.*: 'A theoretical framework for specificity in cell signaling', *Mol. Syst. Biol.*, 2005, **1**, p. 23
19 Zou, X., Peng, T., Pan, Z.: 'Modeling specificity in the yeast MAPK signaling networks', *J. Theor. Biol.*, 2008, **250**, (1), pp. 139–155
20 Wu, F.X., Wu, L., Wang, J., *et al.*: 'Transittability of complex networks and its applications to regulatory biomolecular networks', *Sci. Rep.*, 2014, **4**, (4819), p. 1038
21 Schwartz, M.A., Madhani, H.D.: 'Principles of MAP kinase signaling specificity in Saccharomyces cerevisiae', *Annu. Rev. Genet.*, 2004, **38**, pp. 725–748
22 Bardwell, L., Zou, X., Nie, Q., *et al.*: 'Mathematical models of specificity in cell signaling', *Biophys. J.*, 2007, **92**, (10), pp. 3425–3441
23 Friedlander, T., Mayo, A.E., Tlusty, T., *et al.*: 'Evolution of bow-tie architectures in biology', 2014, arXiv:1404.7715v1
24 Tieri, P., Grignolio, A., Zaikin, A., *et al.*: 'Network, degeneracy and bow tie. Integrating paradigms and architectures to grasp the complexity of the immune system', *Theor. Biol. Med. Model.*, 2010, **7**, (32), pp. 1–16
25 Zhang, W., Zou, X.: 'Systematic analysis of the mechanisms of virus-triggered type I IFN signaling pathways through mathematical modeling', *IEEE/ACM Trans. Comput. Biol. Bioinf.*, 2013, **10**, (3), pp. 771–779
26 Tan, J., Pan, R., Qiao, L., *et al.*: 'Modeling and dynamical analysis of virus-triggered innate immune signalling pathways', *PLoS ONE*, 2012, **7**, (10), p. e48114
27 Tan, J., Zou, X.: 'Complex dynamical analysis of a coupled system from innate immune responses', *Int. J. Bifurcation Chaos*, 2013, **23**, p. 1350180
28 Doncic, A., Falleur-Fettig, M., Skotheim, J.M.: 'Distinct interactions select and maintain a specific cell fate', *Mol. Cell*, 2011, **43**, (4), pp. 528–539
29 Li, Y., Yi, M., Zou, X.: 'Identification of the molecular mechanisms for cell-fate selection in budding yeast through mathematical modeling', *Biophys. J.*, 2013, **104**, (10), pp. 2282–2294
30 Li, Y., Yi, M., Zou, X.: 'The linear interplay of intrinsic and extrinsic noises ensures a high accuracy of cell fate selection in budding yeast', *Sci. Rep.*, 2014, **4**, p. 5764
31 Iwasaki, A., Pillai, P.S.: 'Innate immunity to influenza virus infection', *Nat. Rev. Immunol.*, 2014, **14**, (5), pp. 315–328
32 Hopcroft John, E., Karp, *et al.*: 'An $n^{5/2}$ algorithm for maximum matchings in bipartite graphs', *SIAM J. Comput.*, 1973, **2**, (4), pp. 225–231
33 Zhang, W., Zou, X.: 'A new method for detecting protein complexes based on the three node cliques', *IEEE/ACM Trans. Comput. Biol. Bioinf.*, 2015, **2015**, p. 386235
34 Xiao, X., Zhang, W., Zou, X.: 'A new asynchronous parallel algorithm for inferring large-scale gene regulatory networks', *PLoS One*, 2015, **10**, (3), p. e0119294